# The Impact of Cloud Optical Properties on Longwave Radiation in the Arctic

*J. S. Delamere, E. J. Mlawer, and S. A. Clough*
*Atmospheric and Environmental Research, Inc.*
*Cambridge, Massachusetts*

*K. H. Stamnes*
*Stevens Institute of Technology*
*Hoboken, New Jersey*

## Introduction

The surface energy budget of the Arctic is largely controlled by the net flow of solar and terrestrial radiation. Shortwave and longwave radiative fluxes are modulated by the surface properties, the vertical profiles of aerosols, water vapor, and, most importantly, clouds. The influence of a cloud on the surface and top-of-the-atmosphere (TOA) irradiance is controlled by the cloud's physical characteristics, including particle size, shape, phase, vertical location, and amount of condensed water. There are a number of features present in Arctic clouds that distinguish them from clouds at lower latitudes (Pinto 1998; Hobbs and Rangno 1998; Curry et al. 2000), such as the prevalence of thin layers of liquid water in cloud tops at temperatures as low as -31°C, the highly-variable profile of liquid water content and droplet sizes above the cloud base, frequent precipitation of particles from mid-level clouds to low-level clouds, and the occurrence of low-level ice clouds ("diamond dust"), which extend to the surface.

This study addresses the sensitivity of longwave radiative fluxes to a cloud's optical properties for a particular winter-cloud case occurring during the Surface Heat Budget of the Arctic Ocean (SHEBA) project. We also address the significance of multiple scattering in longwave radiative transfer calculations. While scattering dominates absorption of solar radiation by clouds, the opposite is true in the longwave spectral region. For this reason, scattering, a computationally expensive component of the radiative transfer equation, is often omitted in general circulation model (GCM) longwave radiative transfer calculations. Recent studies (Fu et al. 1997; Chou et al. 1999) suggest that multiple scattering can add an additional 8 $W/m^2$ to the outgoing, TOA flux for a cloudy, mid-latitude summer atmosphere.

## Model Description

To study the sensitivity of radiative fluxes to the optical properties of Arctic clouds, we employed the rapid radiative transfer model (RRTM) (Mlawer et al. 1997) with additional capabilities. RRTM accurately and efficiently calculates vertical profiles of radiative fluxes and heating rates for the longwave spectral region (10 cm to 3000 cm-1, 16 spectral bands) for arbitrary clear atmospheres. RRTM employs the correlated-k technique for radiative transfer, for which molecular k-distributions are

attained directly from the line-by-line radiative transfer model (LBLRTM) (Clough et al. 1992; Clough and Iacono 1995). LBLRTM has been extensively validated against high-resolution radiance measurements.

RRTM now has the option to solve the radiative transfer equation with and without scattering. The discrete-ordinate method algorithm (DISORT) (Stamnes et al. 1988), which fully accounts for multiple-scattering processes, is used to solve the radiative transfer equation for this study.

RRTM is also capable of computing radiative fluxes for cloudy atmospheres. Liquid water cloud radiative properties are calculated with the Hu and Stamnes (1993) parameterization. The extinction coefficient, the single-scattering albedo, and the asymmetry parameter are parameterized as a function of liquid water content and equivalent cloud droplet radius. Ice cloud radiative properties are calculated with the Fu et al. (1998) parameterization. The scheme assumes the ice crystals in the cloud are randomly oriented and hexagonal. Utilizing properties from Mie theory, anomalous diffraction theory, and geometric optics, the parameterization calculates the cloud optical properties as a function of ice water content and generalized effective size (Figure 1).

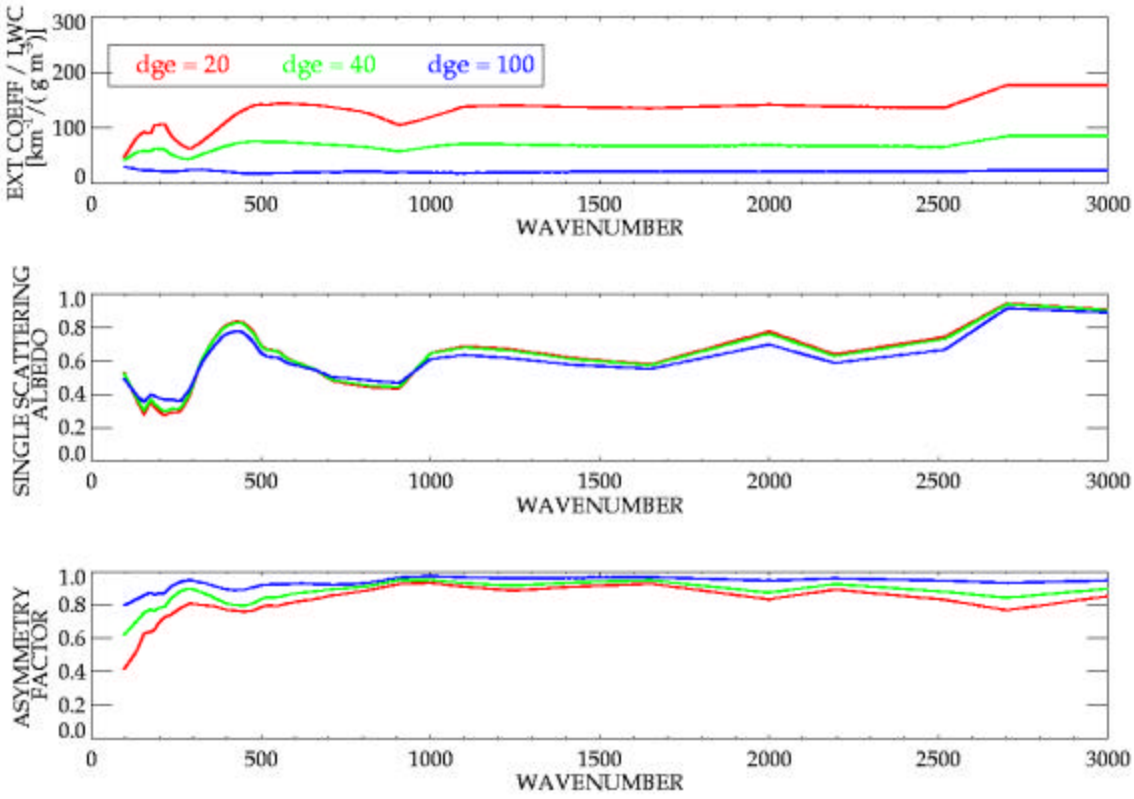


**Figure 1**. Ice cloud properties, computed with the Fu et al. (1998) parameterization, for three particle sizes.

# Case Study Description

For our sensitivity study we used the November 25, 1997, atmospheric profile above the SHEBA station (Figure 2). At this time of year, there is no available solar energy. There were three cloud layers present during the time period for this study: a lower level ice cloud (C1) with a thin layer of water embedded in its top (C2), and an upper level ice cloud (C3) (Figure 3, Table 1). The vertical profile of water content and particle size were assumed to be homogeneous and were set to characteristic values for the baseline case. The surface has been given an emissivity of one for the study.

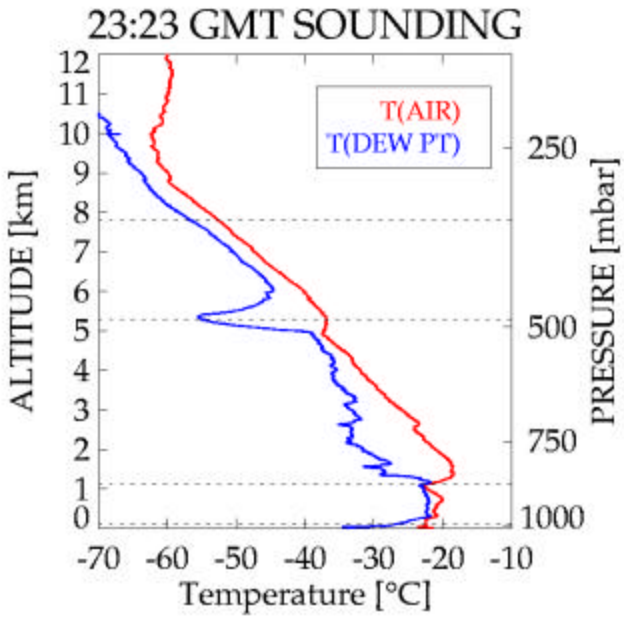


**Figure 2**. Atmospheric temperature and dew point profile over the SHEBA site, November 25, 1997, 23:23 Greenwich Mean Time (GMT). The vertical extents of the clouds are denoted by the dotted lines.

## Sensitivity of TOA and Surface Flux to Particle Size

Setting the water contents to their baseline values, the sensitivity of TOA and surface (SFC) fluxes to changes in particle size was calculated individually for each cloud layer (C1, C2, C3). (Note: The other two cloud layers were simultaneously turned off for the calculation). Results are shown in the left panel of Figure 4 for the three individual cloud layers. TOA flux increases with increasing particle size while the surface flux decreases with increasing particle size. The right panel of Figure 4 illustrates the effect of omitting scattering in the radiative transfer calculations (that is, the mass extinction coefficient equals only the mass absorption coefficient) for the same three scenarios. The largest error, up to 4 $W/m^2$ for the mid-level cloud, occurs when the particle size is smallest for both TOA and SFC flux. Note that with the particular value of water content chosen for these cases, the individual clouds do not reach the optically thick limit.

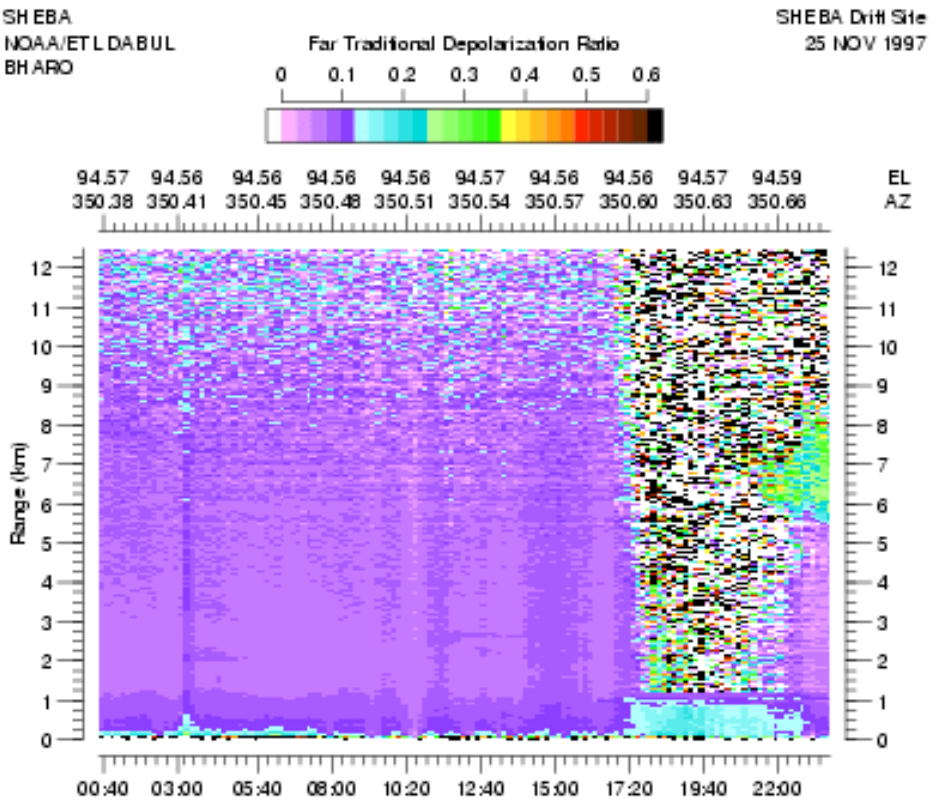


**Figure 3**. Depolarization ratio, measured by the DABUL (Depolarization and Backscattered Unattended Lidar) at SHEBA, shows existence of low-level and mid-level cloud at the approximate time of the sounding in Figure 1.

**Table 1**. Cloud characteristics of baseline case.

| Cloud Name | Altitude [km] | Liquid Water Content [g/m$^3$] | Droplet Effective Radius [mm] | Ice Water Content [g/m$^3$] | Ice Generalized Effective Size [mm] |
|---|---|---|---|---|---|
| C1 | 0.1 - 1.0 | - | - | 0.003 | 40.0 |
| C2 | 0.9 - 1.1 | 0.01 | 7.0 | - | - |
| C3 | 5.3 - 7.8 | - | - | 0.003 | 40.0 |

## Sensitivity of TOA and Surface Flux to Water Content

Setting the particle sizes to their baseline values, the sensitivity of TOA and SFC flux to changes in water content were calculated individually for each cloud layer (C1, C2, C3). (Note: The other two cloud layers were simultaneously turned off for the calculation). Results are shown in the left panel of Figure 5. TOA flux decreases with increasing water content while SFC flux increases with water content. This is expected, since the extinction coefficient is proportional to the water content for both the liquid and ice parameterization. The right panel of Figure 5 again illustrates the impact of multiple scattering on the fluxes for the three scenarios. The maximum error typically occurred when the cloud was neither in the optical thin or thick limit.

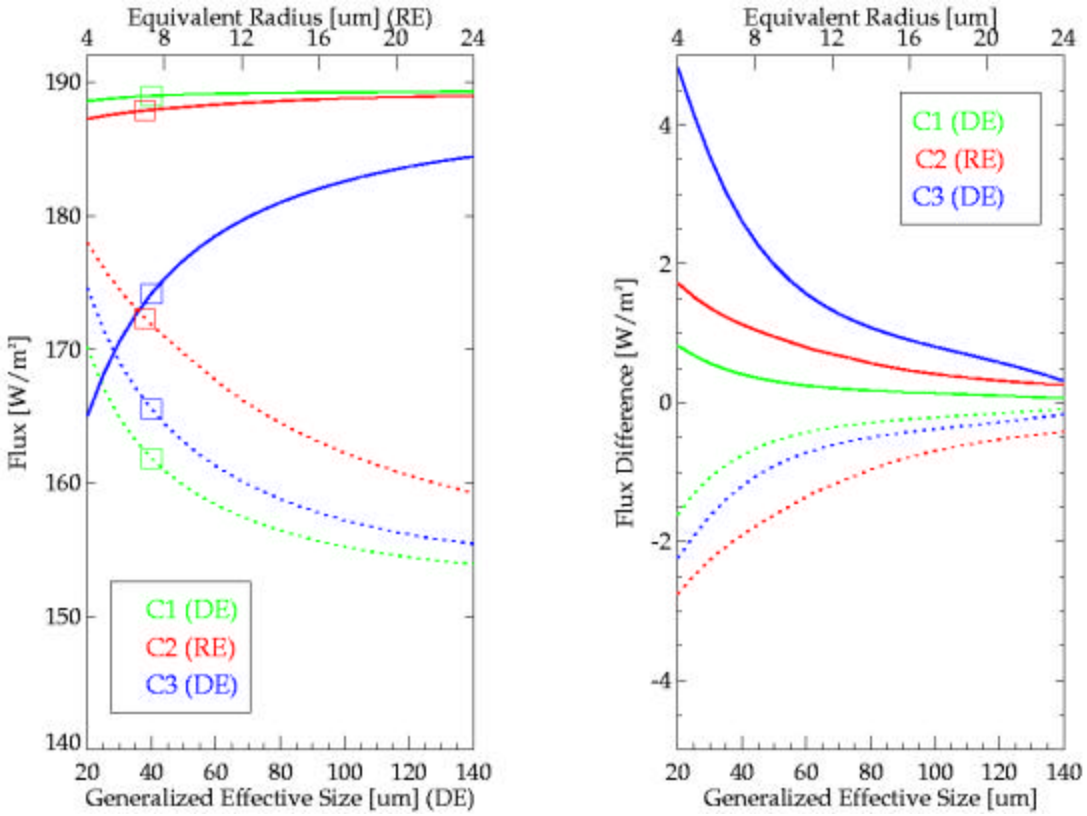


**Figure 4**. Left panel: With water content fixed for each cloud layer, the sensitivity of outgoing TOA flux and downwelling SFC to particle size were calculated for each individual cloud lay (C1, C2, C3) in the baseline case. (Note: For each simulation, the other two cloud layers were simultaneously omitted). The small boxes represent the baseline values of flux. The particle sizes of the ice cloud cases (C1 and C3) are labeled generalized effective size (DE, lower-x axis) while the particle sizes of the liquid water cloud case (C2) are labeled equivalent radius (RE, upper-x axis). Right panel: Differences are plotted between radiative transfer calculations without and with scattering processes for TOA and SFC flux

## Vertical Profile of Radiative Fluxes and Cooling Rates

Vertical profiles of upwelling and downwelling flux and the heating rate for the baseline case are plotted in the left panels of Figures 6 and 7. Since the clouds in the baseline case are not optically thick, the heating rates at cloud top are not as large as would be expected for a typical cloud. Perturbations of the radiative fluxes and heating rates from the baseline case are plotted in the middle and right panels of Figures 6 and 7. In this scenario, each cloud layer (C1, C2, C3) is individually removed, while the other two cloud layers remain. This demonstrates the importance of correctly characterizing each cloudy layer present. The most important conclusion drawn from this calculation is that a thin liquid water layer embedded at the top of an optically thin ice cloud substantially impacts the downwelling flux (15 $W/m^2$ at the surface) and the low-level, cloud top heating rate.

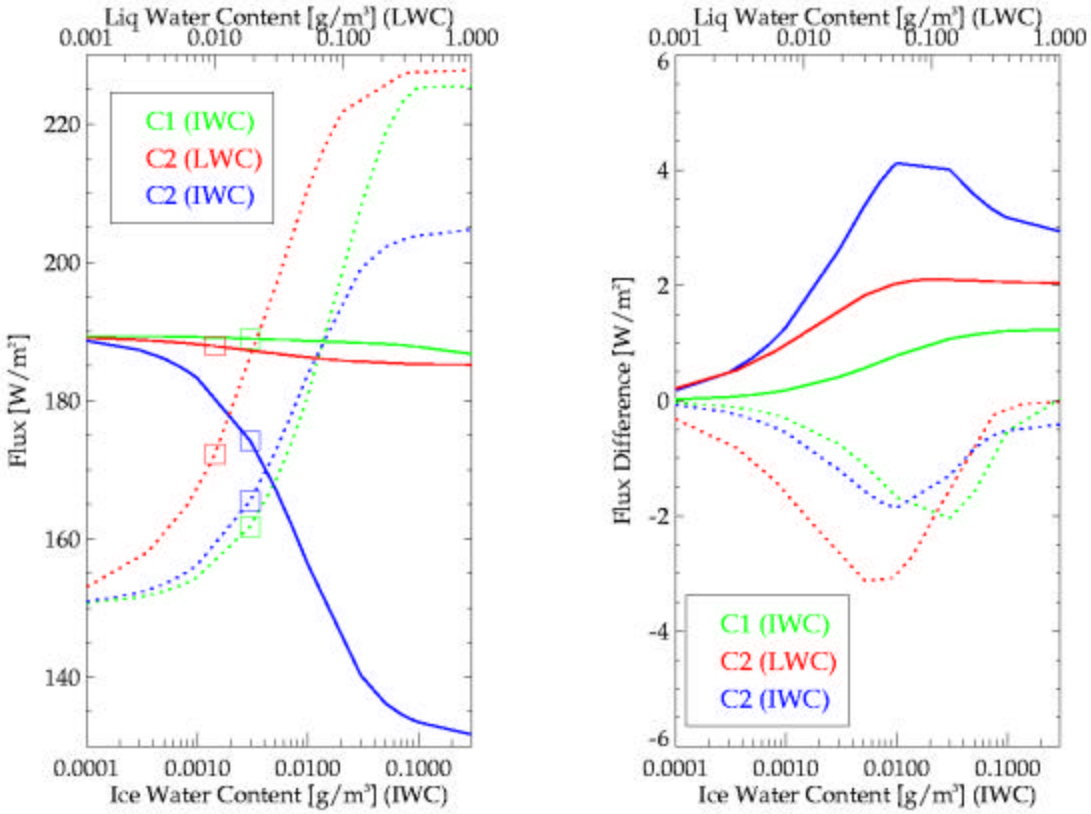


**Figure 5**. Left panel: With particle sizes fixed for each cloud layer, the sensitivity of outgoing TOA flux and downwelling SFC to water content were calculated for each individual cloud layer (C1, C2, C3) in the baseline case. (Note: For each simulation, the other two cloud layers were simultaneously omitted). The small boxes represent the baseline values of flux. The water contents of the ice cloud cases (C1 and C3) are labeled ice water content (lower-x axis) while the water contents of the liquid water cloud cases (C2) are labeled liquid water content (upper-x axis). Right panel: Differences are plotted between radiative transfer calculations without and with scattering processes for TOA and SFC flux.

## Spectral Cloud Forcing

Using the baseline calculation, the baseline-case cloud forcings (Table 2) at TOA and SFC were calculated for each spectral band of RRTM. Downwelling spectral radiation measurements during the Arctic winter have revealed a window region, known as the Arctic window, from 400 $cm^{-1}$ to 600 $cm^{-1}$. The cold, near-surface temperatures, and the low water vapor concentrations significantly reduce clear-sky radiative downwelling fluxes in the low-frequency water vapor rotation bands. In Figure 8, the multiple scattering spectral calculation is overlaid on the absorption spectral calculation to illustrate that multiple scattering effects are particularly important not only in the primary atmospheric window (800 $cm^{-1}$ to 1200 $cm^{-1}$) but also in the Arctic window (400 $cm^{-1}$ to 600 $cm^{-1}$).

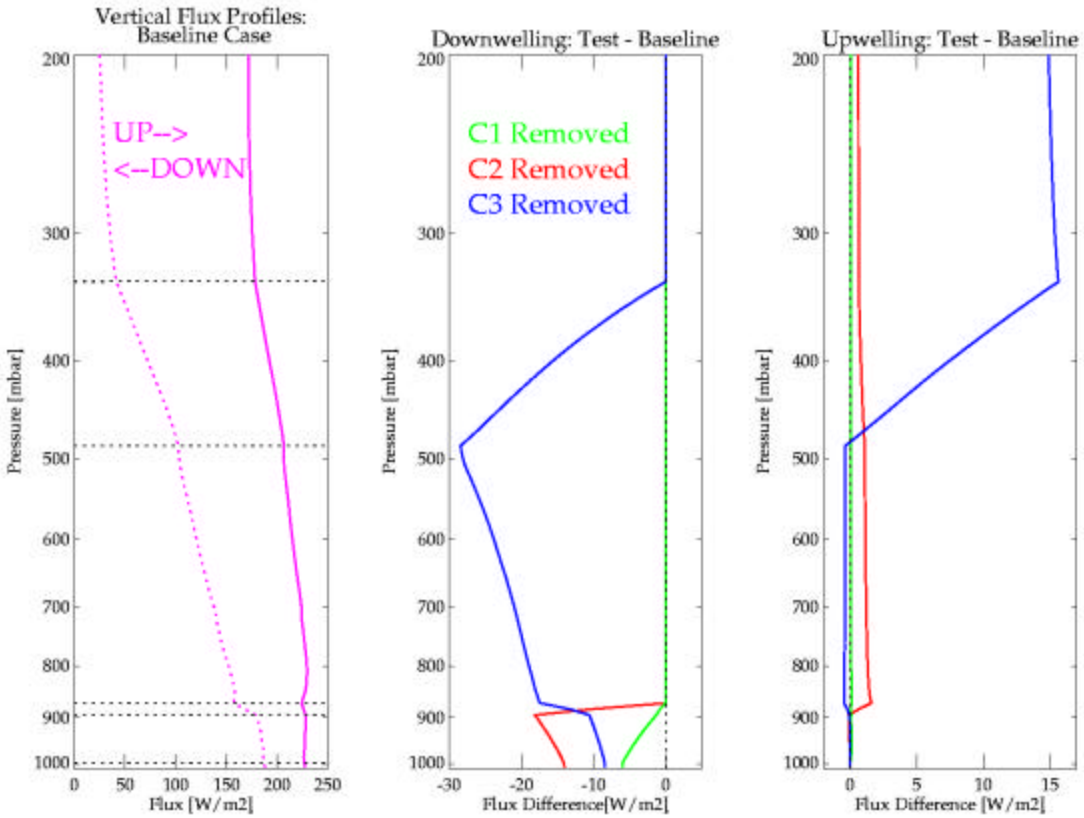


**Figure 6**. Vertical fluxes for the baseline calculation are plotted in the left panel. The dotted line in the left panel illustrates the thickness of each layer. The middle and right panel show flux differences when each of the three individual cloud layers (C1, C2, C3) is removed from the atmospheric profile. (Note: The other two cloud layers are present for the calculation.)

**Table 2**. Total flux and total cloud forcing for the baseline case, with and without scattering included.

| | SFC Flux ($W/m^2$) | SFC Cloud Forcing ($W/m^2$) | TOA Flux ($W/m^2$) | TOA Cloud Forcing ($W/m^2$) |
|---|---|---|---|---|
| Clear | 150.3 | | 189.4 | |
| Absorption Only | 185.8 | 35.5 | 176.6 | -12.8 |
| Multiple Scattering | 188.2 | 37.9 | 173.4 | -16.0 |

## Discussion

We have presented a study of the sensitivity of radiative fluxes and heating rates to changes in the physical properties of Arctic clouds for a winter case over the SHEBA site. The most important conclusion of this study is that thin water layers at the top of a glaciated cloud must be properly characterized to correctly simulate downwelling surface fluxes. This presents a measurement challenge at the U.S. Department of Energy's Atmospheric Radiation Measurement (ARM) North Slope of Alaska (NSA) site, where this phenomenon is likely to occur. In addition, accurate measurements of liquid and

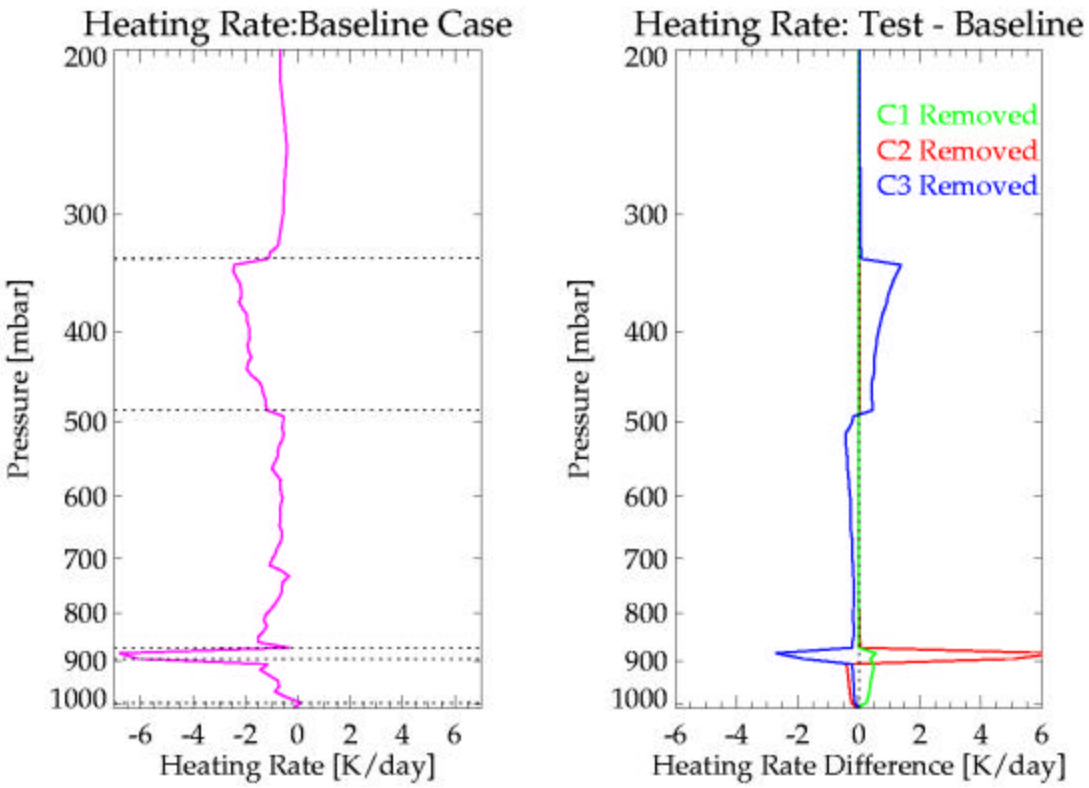


**Figure 7**. Vertical heating rates for the baseline calculation are plotted in the left panel. The dotted line in the left panel illustrates the thickness of each layer. The right panel shows heating rate differences when each of the three individual cloud layers (C1, C2, C3) is removed from the atmospheric profile. (Note: The other two cloud layers are present for the calculation.)

ice water content are crucial for simulating both upwelling and downwelling fluxes. Surface cloud forcing in the presence of a thin layer of diamond dust can exceed 40 W/m2. This again poses measurement challenges in the cold, dry environment of an Arctic winter.

The importance of including multiple scattering in the thermal regime is underscored in this study. Depending on the cloud scene, omitting multiple scattering overestimates the TOA flux and underestimates the SFC flux. These results are consistent with previous studies done at lower latitudes.

## Corresponding Author

Jennifer S. Delamere, jdelamer@aer.com, (617) 349 2298.

## Acknowledgements

Data from the SHEBA campaign was obtained from the SHEBA data archive (ftp://www.joss.ucar.edu), also accessed through the SHEBA Web site (http://sheba.apl.washington.edu).

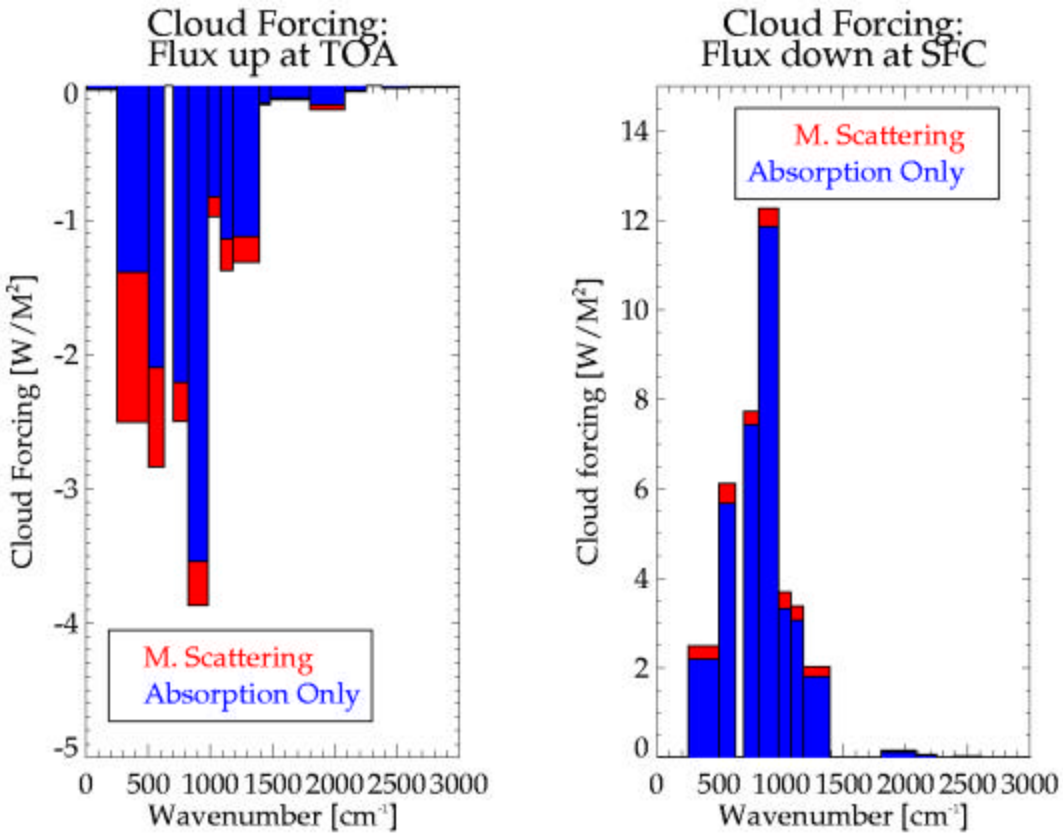


**Figure 8**. Using the baseline calculation, the TOA and SFC cloud forcing (cloudy flux-clear flux) is plotted for the 16 bands of RRTM for the multiple scattering calculation (blue) and no multiple scattering calculation (red).

## References

Chou, M. D., K. T. Lee, S. C. Tsay, and Q. Fu, 1999: Parameterization for cloud longwave scattering for use in atmospheric models. *J. Climate*, **12**, 159-169.

Clough, S. A., M. J. Iacono, and J.-L. Moncet, 1992: Line-by-line calculations of atmospheric fluxes and cooling rates: Application to water vapor. *J. Geophys. Res.*, **97**, 15,761-15,785.

Clough, S. A., and M. J. Iacono, 1995: Line-by-line calculations of atmospheric fluxes and cooling rates 2: Application to carbon dioxide, ozone, methane, nitrous oxide, and the halocarbons. *J. Geophys. Res.*, **100**, 16,519-16,535.

Curry, J. A., P. V. Hobbs, M. D. King, D. A. Randall, P. Minnis, G. A. Isaac, J. O. Pinto, T. Uttal, A. Bucholtz, D. G. Cripe, H. Gerber, C. W. Fairall, T. J. Garrett, J. Hudson, J. M. Intrieri, T. Jensen, P. Lawson, D. Marcotte, L. Nguyen, P. Pilewskie, A. Rangno, D. C. Rogers, B. Strawbridge, F. P. J. Valero, A. G. Williams, D. Wylie, 2000: FIRE Arctic Clouds Experiment, *Bulletin of the American Meteorological Society*, **81**, 5.

Fu, Q., K. N. Liou, M. C. Cribb, T. P. Charlock, and A. Grossman, 1997: Multiple scattering parameterization in thermal infrared radiative transfer. *J. Atmos. Sci*., **54**, 2799.

Fu, Q., P. Yang, and W. B. Sun, 1998: An Accurate parameterization of the infrared radiative properties of cirrus clouds for climate models. *J. Climate*, **11**, 2223.

Hobbs, P. V., and A. L. Rangno, 1998: Microstructures of low and middle-level clouds over the Beaufort Sea. *Q. J. R. Meteorol Soc*., **124**, 2035.

Hu, Y. X., and K. Stamnes, 1993: An Accurate parameterization of the radiative properties of water clouds suitable for use in climate models. *J. Climate*, **6**, 728.

Mlawer, E. J., S. J. Taubman, P. D. Brown, M. J. Iacono, and S. A. Clough, 1997: Radiative transfer for inhomogeneous atmospheres: RRTM, a validated correlated-k model for the longwave. *J. Geophys. Res*., **102**, 16,682.

Pinto, J. O., 1998: Autumnal mixed-phase cloudy boundary layers in the Arctic. *J. Atmos. Sci*., **55**, 2016.

Stamnes, K., S. C. Tsay, and W. Wiscombe, 1988: Numerically stable algorithm for discrete-ordinate method in multiple-scattering and emitting layered media. *Appl. Opt*., **27**, 2502.